Granular Matter (2007) 9:365–376
DOI 10.1007/s10035-007-0050-6

Attenuation in sand: an exploratory study on the small-strain behavior and the influence of moisture condensation

Y.-H. Wang · J. C. Santamarina

Received: 23 December 2005 / Published online: 1 August 2007
© Springer-Verlag 2007

Abstract The loss mechanisms responsible for the observed attenuation in soils are often unclear and controversial. This is particularly the case with the small-strain damping $D_{\min}$ in air-dry sands. Ultimately, physical explanations must accommodate the observed effects of confinement, strain level, frequency, and load repetition. Three hypotheses are explored herein: measurement bias, thermoelastic relaxation, and adsorbed layers. Micro and macroscale experimentation using photoelasticity, thermal infrared imaging, atomic force microscopy and resonant column testing are complemented with conceptual analyses. Results show that Mindlin-contact friction cannot explain the observed response of the small-strain damping ratio $D_{\min}$ and thermoelastic loss is suggested. While thermoelastic relaxation is inherently frequency dependent, the superposition of multiple internal scales in soils can justify the observed low dependency on frequency. Moisture condensation leads to adsorbed water layers on grain surfaces, which has a small but observable effect on shear modulus and a significant influence on damping ratio. Participating loss mechanisms at small-strains may involve distortion and motion of adsorbed layers and hydration force hysteresis. Hysteretic capillary breakage at contacting asperities gains relevance when the strain exceeds the elastic threshold strain; this strain coincides with the strain range when frictional losses begin to dominate. Finally, the damping ratio in air-dry sands is very small, and causality-based attenuation–dispersion relations predict modulus dispersion about 1% per log cycle, therefore the medium can be considered non-dispersive for practical purposes.

Keywords Damping ratio · Sands · Microscale · Capillary force · Resonant column · AFM · Thermoelasticity · Counter emf · Relative humidity

Y.-H. Wang (✉)
Department of Civil Engineering,
The Hong Kong University of Science and Technology,
Clear Water Bay, Kowloon, Hong Kong
e-mail: ceyhwang@ust.hk

J. C. Santamarina
Department of Civil and Environmental Engineering,
Georgia Institute of Technology, 790 Atlantic Drive,
Atlanta, GA 30332, USA
e-mail: carlos.santamarina@ce.gatech.edu

1 Introduction

Soils cannot vibrate freely forever because energy dissipation always takes place. Thus, attenuation is an inherent soil characteristic. It determines the peak response of soil near resonance (amplification = 1/2 D, where D is the damping ratio of soil; [22,47]), has a strong effect on ground amplification during earthquake [78], affects reservoir characterization [44], and provides complementary information about the behavior of the soil that is not revealed by stiffness measurements (examples in [16,51]).

The analysis of published small-strain data for air-dry sands shows contradictory observations. For example, frictional loss is the most accepted energy loss mechanism for dry sands. In agreement with this hypothesis, published data show that the small-strain damping ratio $D_{\min}$ decreases with effective confinement (classical data in [32]). However, while frictional loss should vanish as the strain diminishes $\gamma \to 0$, experimental results show that the damping ratio approaches a constant, not-null value at small stains, i.e., $D \to D_{\min}$. Furthermore, $D_{\min}$ is not affected by the number of loading cycles [51], even though the oscillating force, which can produce surface damage, i.e., fretting, would alter the frictional loss [23,40]. If friction is discarded as a small-strain

energy loss mechanism, then other loss mechanisms must be considered to simultaneously explain all the available experimental data.

This unclear situation is also observed in relation to moisture effects. Materials tested under especially dry conditions exhibit a significantly lower $D_{\min}$ than the same materials under moist-air condition (for an interesting case, consider data gathered by the Apollo 12 mission in [49,74,75]). While the available data suggest—albeit not conclusively—that even few monolayers of adsorbed water can play an important role in energy loss, associated loss mechanisms remain unclear.

This study is designed to elucidate the above predicaments, with emphasis on the attenuation characteristics of air-dry sands at small strains, i.e., $D_{\min}$. It begins with a brief review of fundamental concepts related to attenuation and general trends regarding the influence of various factors on the small-strain dynamic properties of soils. Then, three hypotheses are analyzed to explain observed losses: measurement bias, thermoelastic relaxation in the context of particulate media, and hysteretic effects in moist sands. These hypotheses are explored through a combination of particle-level and macro-scale experimental studies and complementary conceptual analyses (Complete test sequences, data sets and detailed reviews and analyses can be found in [80]).

2 Preliminary concepts

Attenuation in wave propagation is the decay of the wave amplitude away from the source. The total attenuation arises from geometric spreading, apparent attenuation, and material losses. Geometric spreading takes place in non-planar wave propagation and reflects the increasing size of the wave front. Apparent attenuation is due to partial transmission, mode conversion, diffraction, and scattering at interfaces and anomalies. Finally, material losses arise due to energy transformation into other forms, ultimately becoming heat. This study addresses material losses.

In soil mechanics, material losses are quantified with the damping ratio $D = W_L/4\pi W_S$, which compares energy loss W_L and the maximum stored energy W_S per cycle. Other quantities are used to represent attenuation, such as the quality factor Q, the logarithmic decrement $\delta_{\log}$, and the attenuation coefficient α. The following equality between these parameters applies to low-loss conditions [67]:

$$D \equiv \frac{W_L}{4\pi W_S} = \frac{Q^{-1}}{2} = \frac{\delta_{\log}}{2\pi} = \frac{\lambda\alpha}{2\pi} = \frac{1}{2\pi} V\, f\, \alpha \tag{1}$$

Parameters in Eq. 1 include the wavelength λ, frequency f, and wave velocity V.

In general, material losses can be categorized into two types. One category is frequency-dependent "linear" losses (i.e., viscous losses), typically caused by the viscous pore fluid and internal energy coupling such as anelastic relaxations. The other category includes displacement-dependent and frequency-independent "non-linear" losses; typically, this is the case of frictional loss occurring at contact points between grains, cracks and interfaces. The two types of mechanisms coexist and determine the measured material damping.

Many factors associated with different loss mechanisms affect the damping ratio in geomaterials; these include: frequency of the propagating perturbation, effective confinement, strain level, degree of saturation, fluid properties, and various properties of the granular medium such as porosity, gradation, grain shape, fabric structure, material properties of individual grains and clay content among others [24,31,41,56,84]. Table 1 summarizes the most important factors that affect the small-strain (or the minimum) damping ratio $D_{\min}$ in soils; for completeness, the impact of these factors on the small-strain (or the maximum) shear modulus $G_{\max}$ is discussed as well. These trends are based on experimental observations; some underlying mechanisms are explored in this study.

The strain level significantly affects the dynamic properties of soils. Figure 1 depicts salient characteristics of the

Table 1 Soil factors that affect the small-strain dynamic properties $G_{\max}$ and $D_{\min}$

"Increasing" Factors	The maximum shear modulus $G_{\max}$		The minimum damping ratio $D_{\min}$	
	Sands	Clays	Sands	Clays
Strain	Quasi constant (decisive decrease as $\gamma > \gamma_{tl}$)		Quasi constant (decisive increase as $\gamma > \gamma_{tl}$)	
Confining pressure, σ'	Increases with σ'		None/slight decrease with σ'	
Degree of saturation, S	Decreases with S[a]		Non monotonic variation with saturation	
Preloading	Isotropic: Slight-none, K_o: function of OCR	Increases with OCR	Slight or no effect	Decreases with OCR
Aging time, t	Increases with t		Decreases with t	
Cementation, c	High increase with c	Increase with c[b]	Inconclusive	May decrease with c

Note: [a] Caution: depends on drying-wetting history
[b] Cemented, high void ratio natural clays may exhibit higher stiffness after remolding and reconsolidation (same stress level but lower void ratio)
Sources: [24,31,36,42,46,51,79]; Santamarina and coworkers including results presented in this paper

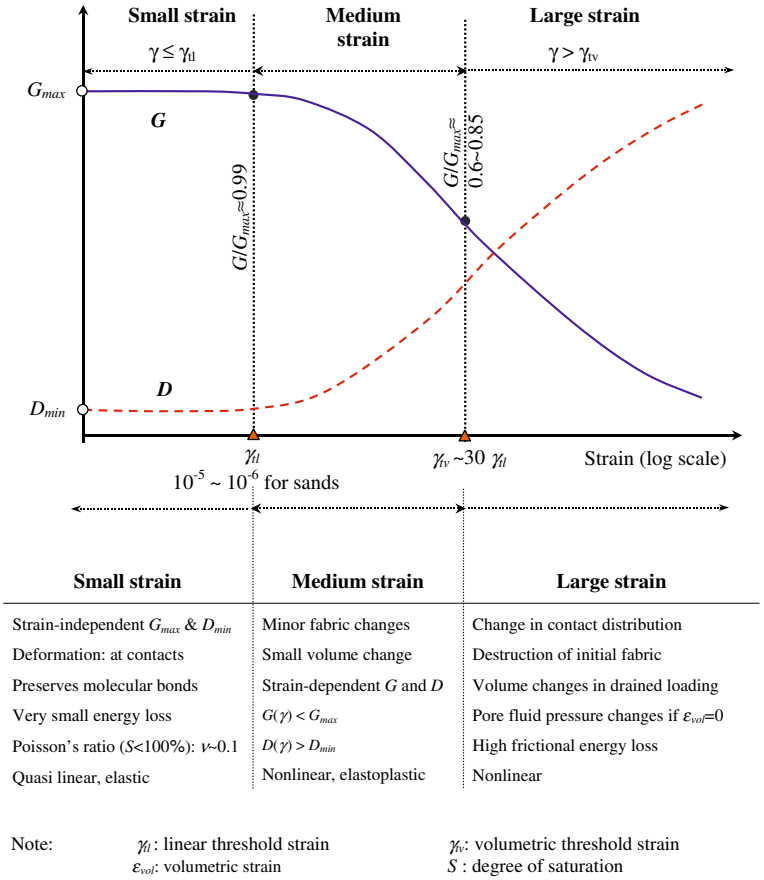

Fig. 1 Characteristics of shear modulus and damping ratio of soils at different strain levels (based on: [36,47,69,79])

damping ratio D and shear modulus G at different strains. The damping ratio and shear modulus become strain-dependent when the strain level exceeds the linear threshold strain ($\gamma > \gamma_{tl}$). The linear threshold strain in sands is $\gamma_{tl} \sim 10^{-5}$ to 10^{-6}. Different techniques of the damping ratio and shear modulus measurements can be found in [69].

3 Frictional loss reconsidered

Most damping-ratio measurements in geotechnical engineering are implemented in resonant column devices, where a cylindrical specimen is subjected to effective confinement and excited in torsion. The cylindrical shape and the long wavelength standing wave (multiple of the specimen height [36]) prevent geometric spreading and scattering. Therefore, in principle, the measured damping ratio reflects only the material loss. However, inherent biases in the measurements may affect data interpretation; this situation is investigated first.

3.1 Measurement bias

Resonant column testing data is affected by experimental difficulties and inversion assumptions such as: energy leak from the assumed "fixed-boundary" as impedance mismatch diminishes (typically in stiff specimens—[6]), shear strain gradient across the radius, and the assumption of constant damping around the resonant frequency. In general, these effects can be neglected at small strains ($\sim \gamma \leqslant 10^{-5}$) and at typical resonant frequencies attained in near-surface soil studies.

Of particular interest for this study of dry sands is another measurement bias known as the counter emf effect [18,42,57]. This effect results from the relative displacement between magnets and driving solenoids during cyclic loading: the magnetic field generated by the magnets causes a changing magnetic flux through the coils and an electromotive force emf that opposes the motion. This inherent counter-excitation in coil-magnet systems introduces an additional "virtual inertia" I_{emf} and "electrical damping" c_{emf} to the testing system [81],

$$I_{emf} = \frac{a \cdot L}{R_\Omega^2 + \omega^2 L^2} \tag{2}$$

$$c_{emf} = \frac{a \cdot R_\Omega}{R_\Omega^2 + \omega^2 L^2} \tag{3}$$

where R_Ω and L are the resistance and inductance of the coils, ω is the angular frequency, and a is an equipment related constant that is readily obtained from calibration. The values of

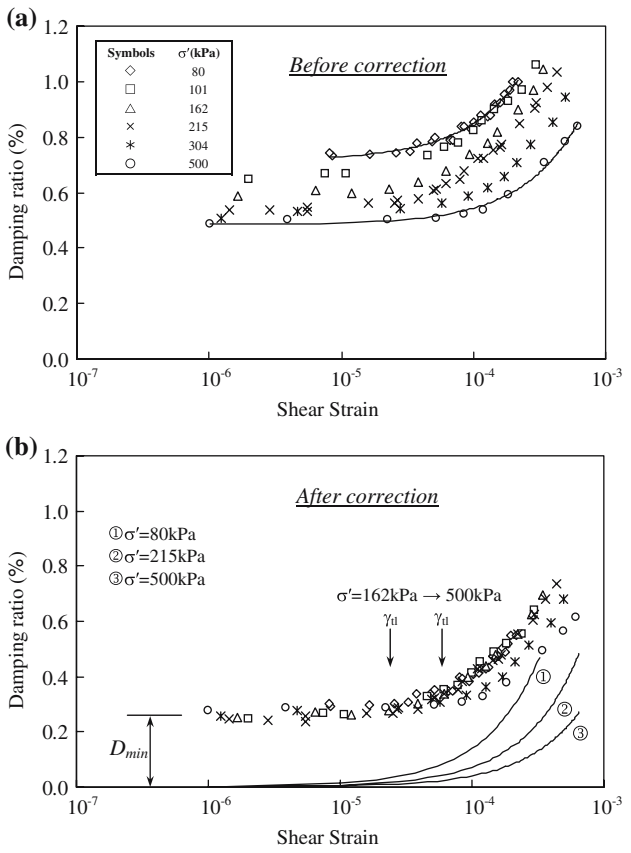

Fig. 2 Experimental bias—Counter emf effect. **a** Original data before correction (from [68]). **b** Corrected data. Solid lines are the theoretical predictions based on Mindlin's contact model (Eqs. 4 and 5: $f_s = 0.85$, $\nu = 0.35$, $E = 2.8$ GPa)

I_{emf} and c_{emf} affect both the measured shear modulus and damping ratio. The correction of $G_{\max}$ is very small and can be disregarded. However, the counter emf effect can overshadow the material damping ratio, especially for dry sand specimens under low confinement [81].

Figure 2 shows the damping ratio measured for dry sands before and after correction for the counter emf effect. While the uncorrected data show that $D_{\min}$ is confinement-dependent, the corrected data show almost no confinement-dependence. Therefore, frictional loss is not justified by corrected $D_{\min}$ data. A physical analysis of frictional loss is attempted next, before frictional loss is discarded in the small-strain regime $\gamma < \gamma_{tl}$.

3.2 Measured versus predicted trends

Let's assume a simple cubic packing of elastic spherical particles interacting through Hertz–Mindlin type contact [40]. In this case, the surface roughness is not considered and the energy loss results from micro-slip at contact annuli. The strain and confinement-dependent damping ratio D is [25]

$$D = \frac{12}{5\pi}\left\{\frac{1-\left(1-\frac{\gamma}{\gamma_m}\right)^{5/2}}{\frac{\gamma}{\gamma_m}\left[1-\left(1-\frac{\gamma}{\gamma_m}\right)^{3/2}\right]} - \frac{5\left(2-\frac{\gamma}{\gamma_m}\right)}{6\frac{\gamma}{\gamma_m}}\right\}$$

which becomes

$$D \approx \frac{1}{6\pi}\frac{\gamma}{\gamma_m} \text{ for } \frac{\gamma}{\gamma_m} \to 0 \tag{4}$$

where γ is the shear strain and the Mindlin strain γ_m at gross particle sliding is

$$\gamma_m = 2.08\frac{(2-\nu)(1+\nu)f_s\sigma'^{2/3}}{(1-\nu^2)^{1/3}E^{2/3}} \tag{5}$$

and f_s is the interparticle friction coefficient, E and ν are the Young's modulus and Poisson's ratio of the material that makes the particle, and σ' is the isotropic confining pressure. Trends predicted with this model are superimposed on Fig. 2b; it is seen that the predicted damping ratio tends to zero at small-strains $D \to 0$, rather than the experimentally observed $D \to D_{\min}$. If predicted values are increased by $D_{\min}$, the model approaches the data. This suggests that energy loss is preponderantly frictional above the linear threshold strain γ_{tl}, but not at small-strain.

At the particle level, repeated loading causes fretting at contacts [39]; increases the friction coefficient in the micro-slip zone and enlarges the stick regime [23]. At the macro-scale, fretting ensuing skeletal changes when $\gamma > \sim\gamma_{tl}$ increase the shear modulus and decrease the damping ratio; however, $D_{\min}$ and $G_{\max}$ remain virtually constant when $\gamma = 10^{-5} < \gamma_{tl}$ even after 10^6 loading cycles ([51] where the system compliance including the counter emf effects are well characterized and eliminated from the measurement). Therefore, the small-strain damping ratio $D_{\min}$ does not respond to cyclic loading effects that are characteristic in large-strain frictional cyclic response.

3.3 Physical limit: summary

There is an inherent limit to strain-dependent frictional loss. Let's assume that all the relative displacements δ between two contiguous particles of size d localizes at the interparticle contact when the soil experiences a strain γ. The resulting contact displacement $\delta = \gamma d$ must exceed the atomic scale $\delta > \sim$Å to cause slippage [68,85]. Therefore, no friction can be justified when the strain level is $\gamma < $ Å$/d$. For example, a 0.1 mm diameter sand subjected to $\gamma = 10^{-6}$ strain experiences a relative displacement between two adjacent particles $\delta \approx 1$Å.

In summary, corrected experimental data and physical limits show that the small-strain damping ratio $D_{\min}$ in dry sands is non-zero, it is relatively independent of confinement, and it is unaffected by the strain level and the number of

loading cycles. This behavior cannot be explained as frictional loss. A non-frictional loss mechanism is explored in the next section.

4 Thermoelastic relaxation—losses in $D_{\min}$

Experimental results with metal spheres suggest that small-strain loss in granular materials results from "anelastic effects" within the particles rather than from micro-slip at contact annuli (see data in [39,40]). Energy loss due to thermoelastic coupling is analyzed next.

4.1 Thermoelastic relaxation in the continuum

Thermoelastic loss has been suggested to account for anelastic effects in a wide range of continuous materials, including dry rocks [4,5,70]. Thermoelastic loss involves:

- Thermal changes caused by stress changes. The thermoelastic coupling combines the thermal expansion coefficient α_t[K^{-1}], the specific heat at constant stress C_σ[J m^{-3}K^{-1}] and the material stiffness B [Pa].
- Heat diffusion. The time scale for heat diffusion τ_{rel} [s] is a function of the length scale d_L [m] from source to boundary, and the thermal diffusivity D_{th} [m^2/s]. It can be estimated as $\tau_{rel} \approx d_L^2/D_{th}$.
- The time scale for the excitation, $T = 2\pi/\omega$ where ω is the excitation frequency.

The process is adiabatic if the duration of the excitation is much shorter than the time scale for heat diffusion ($\omega\tau_{rel} >> 1$—Fig. 3a). On the other hand, the process is isothermal if the duration of the excitation is very long ($\omega\tau_{rel} << 1$) and the material temperature remains constant and homogeneous with the ambient temperature. Thermoleastic hysteresis takes place when the two time scales are similar ($0.1 < \omega\tau_{rel} < 10$).

The damping ratio for thermoelastic loss in a continuum is (assumes low energy loss [90]; see also [62]):

$$D = a_s \frac{B\alpha_t^2 T_0}{C_\sigma} \frac{\omega\tau_{rel}}{1+\omega^2\tau_{rel}^2} \tag{6}$$

where T_0 [K] is the ambient or reference temperature and the factor a_s is related to boundary and initial conditions. Similar expressions apply to beams in flexion or to intercrystalline thermoelastic relaxation in a continuum (e.g., [4,90]). Heterogeneity significantly affects the extent of thermoelastic relaxation, and the relaxation time τ_{rel}.

4.2 Thermoelastic relaxation in soils: experimental study

Equation 6 indicates that thermoelastic-diffusion loss is strain independent and has a relaxation-type spectral response as plotted in Fig. 3b. The first characteristic is in agreement with the small-strain damping ratio $D_{\min}$ in dry sands. However, experimental observations suggest that $D_{\min}$ is fairly constant in frequency [42,52]. As shown in Fig. 3c, it is possible to construct a nearly constant damping ratio response

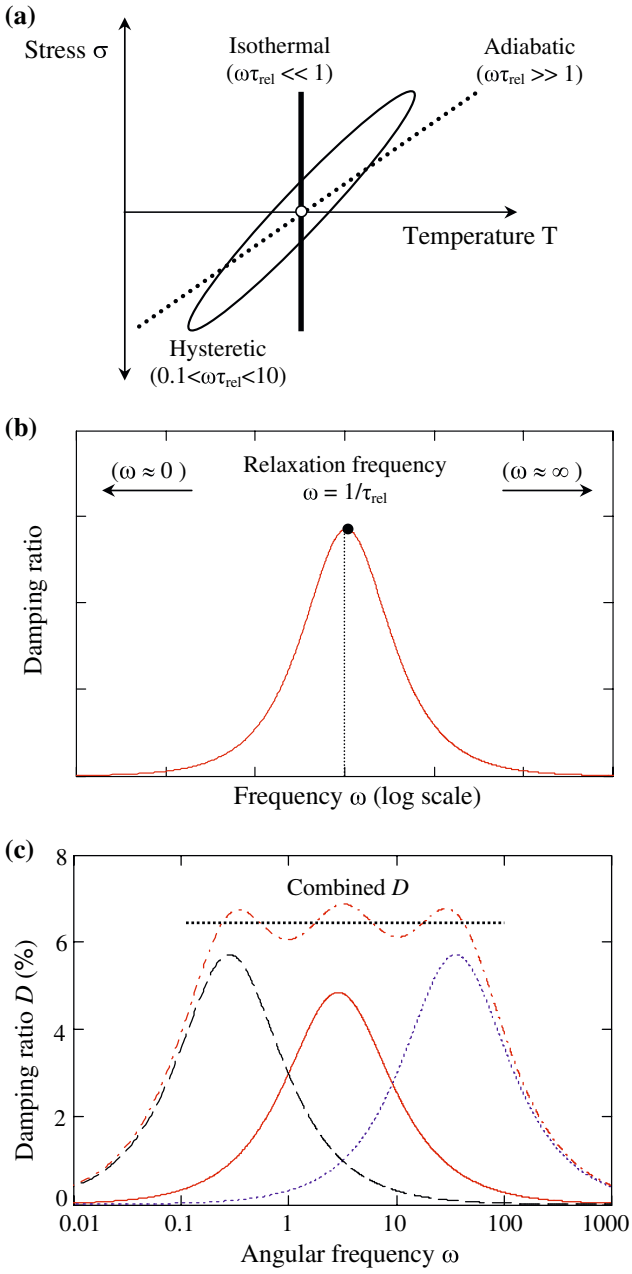

Fig. 3 Frequency effects in thermoelastic losses. **a** Thermoelastic hysteresis. **b** Associated damping ratio spectrum. **c** Nearly-constant damping ratio response by the superposition of multiple relaxations

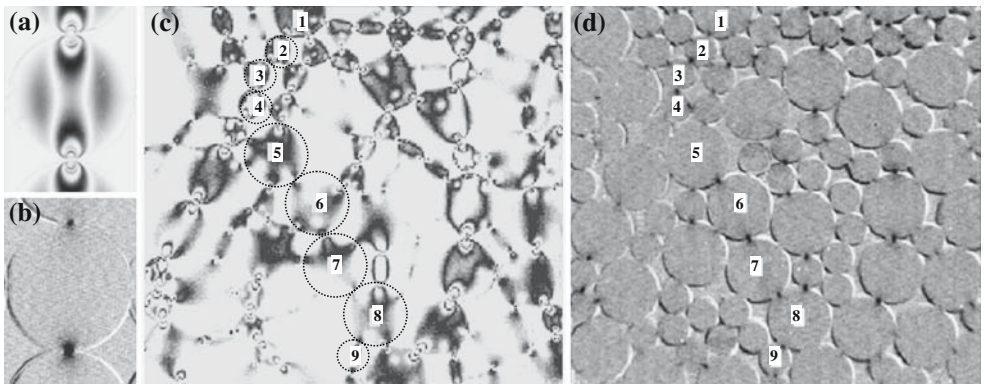

Fig. 4 Multiple internal scales in particulate materials. **a** Photoelastic image of fringe patterns around contacts (contours of principal shear stress). **b** Corresponding IR image under cyclic loading (photoelastic disk diameter $d = 25.4$ mm, Hertzian contact radius $r_c = 0.21$ mm). **c** Photoelastic image for disk packing. **d** Image of the same packing captured by the infrared camera under cyclic loading. The "hot" regions (*black spots*) appear around contacts and follow the trend of force chains—a complete force chain is numbered to facilitate its identification in both images

by the superposition of relaxations with different time scales (a similar strategy is followed by [43,53] in rocks). Therefore, it is herein hypothesized that the observed quasi-constant damping ratio in dry soils at small-strains is the result of multiple coexisting thermoelastic relaxations with different time scales τ_{rel}, which are associated to various internal length scales d_L in soil masses.

This hypothesis is experimentally explored in particle networks by combining photoelasticity and infrared photography. The photoelastic disks are used to simulate a granular packing (PSM-1, Measurement Groups, Inc.—diameters 12.7 and 25.4 mm). The two-dimensional packing is laterally bound by a rigid frame (width: 0.18 m) and is subjected to static vertical loading (line load ~5 N/m). The stress distribution within disks and the force chains in the disk network are captured with a photoelastic camera (GFP1000, Stress Photonics Company). The small thermoelastic effect is detected above the ambient thermal noise by cycling the applied load (0.8 Hz), taking infrared images in phase with the applied excitation (IR camera DT1500, Stress Photonics Company), and stacking 250 images to increase the signal-to-noise ratio.

Figure 4 presents photoelastic and IR images for the network and detailed images of a single disk. The stress field inside particles is characterized by stress concentration at contacts (several fringes are observed around contacts in Fig. 4a; for an exceptional early image see [28]). Thermal changes prevail at contacts (dark points near contacts in Fig. 4b; corroboration with Hertzian contact predictions can be found in [80]. The network exhibits the well known formation of force chains (Fig. 4c) with primarily loaded particles and secondary particles loaded in the transverse direction to prevent the buckling of the main chains [66]. The IR image of the network shows "hot" contacts along the primary force chains, in correspondence with the photoelastic image (Fig. 4d).

Similar observations are gathered from several similar experiments and are expected to be found in a sand packing. The following distinct length scales d_L can be identified for thermal diffusion and the ensuing thermoelastic relaxation during wave propagation:

- The contact or particle scales, whereby thermal changes at the contacts diffuse towards the body of the particle (and into the pore fluid).
- The chain scale. In this case, thermal currents are expected between primary particles involved in the chains and the remaining secondary particles. Note that heat flow in dry particulate media is dominated by conduction rather than radiation or convection [1]. Furthermore, heat flow paths occur through the solid phase because thermal conductivity is higher in minerals than in air. Because force chains have a wide range of internal scales, resembling a fractal structure, one would expect a wide range of relaxation times.
- Finally, a propagating wave imposes a non-homogeneous stress field with opposite peaks $\lambda/2$ apart. Therefore, the wavelength λ is an additional length scale relevant to thermoelastic relaxation (analytical—this is not an experimental observation). In the particular case of resonant column testing, the associated length scale is the specimen length.

These multiple internal spatial scales and the associated thermal diffusion coefficients lead to a wide range of thermoelastic relaxation times $\tau_{rel} \approx d_L^2 / D_{th}$. While the coexistence of dissimilar time scales does not necessarily prove that thermoelastic relaxation is the main loss mechanism behind the small-strain damping ratio of dry sands, $D_{\min}$, these results support the concept that a micro-scale relaxation mechanism can underlie a macro-scale frequency independent damping

ratio in particulate media (within some frequency range of interest).

5 Attenuation due to adsorbed water layers in moist sands

Most minerals are hydrophilic and favor water vapor condensation on their surfaces. The number of adsorbed monolayers N_{ads} depends on the relative humidity RH, as predicted by the BET equation [14],

$$N_{ads} = \frac{c \cdot RH}{(1 - RH)\,[1 + (c - 1) \cdot RH]} \tag{7}$$

where c is a parameter related to the heat of adsorption in the first and subsequent adsorbed layers, gas constant, and absolute temperature. Results predicted with Eq. 7 (using $c = 48.98$) show that the surface is covered with one monolayer at $RH \approx 12\%$ and about 10 monolayers when $RH \geqslant 90\%$.

5.1 Adsorbed water: implications

The following properties and potential implications of adsorbed water are relevant to this study:

- The first few monolayers (typically less than 5–8 monolayers) exhibit different mobility, dielectric constant, and diffusion [21,45,64]. This is caused by the strong influence exerted by the mineral on water molecules and ions; further monolayers behave as bulk free water.
- The first and second adsorbed water monolayers are not readily displaced even at high contact pressure, and reduce the solid-solid contact area [34].
- Adsorbed water molecules are more structured towards the mineral surface [33,37,38,65]. The required approach force oscillates with period equivalent to a monolayer thickness, and a low retreat force is expected. Therefore hysteretic behavior is expected in solvation forces (Note: this is a form of atomic scale "squirt-flow"—it has not been studied).
- Boundary lubrication by adsorbed water layers in hydrophilic mineral surfaces generally reduces interfacial friction with increasing relative humidity [7,8,35]. However, adsorbed water layers may form capillary bridges between contacting asperities and increase the inter-surface normal force so that friction may increase with capillary condensation (e.g., [11]).
- Molecular dynamic simulations show that the structured boundary layers (i.e., the few monolayers attached to the solid surface) go through liquid–solid transitions when sheared [48]. This can explain why friction in the boundary lubrication regime depends on temperature, contact pressure, and relative sliding velocity [89].
- The presence of moisture at contacts effects the thermal diffusion and the thermoelastic relaxation frequency, as it can be deduced by comparing the thermal diffusion of the different soil phases is: $D_{th} = 0.21 \times 10^{-7}\,\mathrm{m^2/s}$ for air, $D_{th} = 1.3 \times 10^{-7}\,\mathrm{m^2/s}$ for water, and $D_{th} = 3\text{-to-}40 \times 10^{-7}\,\mathrm{m^2/s}$ for common soil minerals [1].
- Finally, note that the interparticle deformation concentrates at interparticle contacts. Thus, adsorbed layers experience a much higher strain level than the average strain level imposed on the soil mass.

5.2 Adsorbed water effects in intact rock

The reported macro-scale effects of adsorbed layers on dynamic properties are restricted primarily to rocks (data for soils are either absent or inconclusive). Experimental observations indicate that small-strain attenuation increases with small amounts of water forming adsorbed water films. The breakage of hydrogen bonds, micro-capillary hysteresis (viscous dissipation on rough surfaces combined with the breakage of chemical bonds), and the local flow of condensed water layers have been hypothesized to explain observed results [13,20,45,61,76].

Published small-strain results also show a significant decrease in stiffness with increasing relative humidity for different rocks [20], and other materials such as Vycor porous glass [61]. Matrix softening may result from mineral hydration and changes in electrical forces [20,59].

5.3 Adsorbed water effects in soils: macro-scale experimental study

The effects of adsorbed water layers on the dynamic properties of sand are evaluated using fine-grained sand to amplify any effect ($d_{50} = 125\mu$m, $C_u = 1.76$, $S_s = 0.19\,\mathrm{m^2/g}$—measured with N_2 gas adsorption). A dense sand specimen ($\rho_s = 1.61\,\mathrm{g/cm^3}$) is prepared to prevent fabric changes, and the same specimen is used in all tests to avoid biases. The confining pressure is kept constant at $\sigma' = 69\,\mathrm{kPa}$ for the complete test sequence.

Two extreme cases are compared: dry-air and saturated-air conditions. The relative humidity or moisture status inside the specimen is controlled by gently flowing moisture-conditioned air for several hours. Dry-air is generated by pumping air through a column filled with hydrous $CaSO_4$. The saturated-air is produced by bubbling air through deionized water. At the selected humidity conditions, the damping ratio D and the shear modulus G are measured for different strain levels, using the resonant column technique and a random noise excitation technique with proper correction for counter emf effects (test methodology in [17]; correction procedure in [81]).

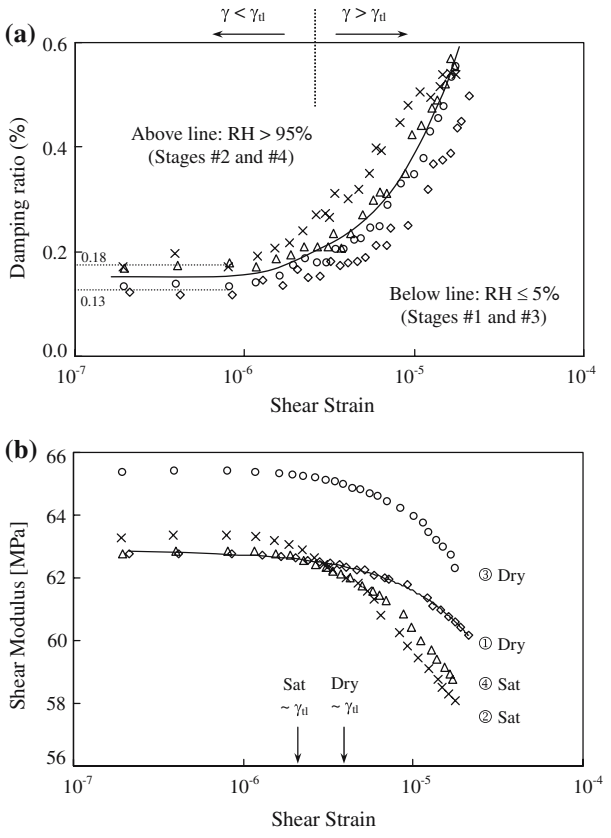

RH	Stage	Symbol	Descriptions
5%	#1	◇	**Dry air:** Flow through dry air for 36 hrs
95%	#2	×	**Saturated air:** Flow through saturated air for 63 hrs
5%	#3	○	**Dry air:** Flow through dry air for 68 hrs
95%	#4	△	**Saturated air:** Flow through saturated air for 56 hrs

Fig. 5 The effect of relative humidity on D and G—Resonant column test. **a** Damping ratio D. **b** Shear modulus G

The following sequence of air moisture stages is imposed: (1) dry, (2) saturated, (3) dry, and (4) saturated. Representative test results are shown in Fig. 5. The following observations can be made:

- The small and middle-strain damping ratio increases as the relative humidity increases. At small-strains $\gamma < \gamma_{tl}$, there is a 38% increase in $D_{\min}$. High relative humidity causes a decrease in the linear threshold strain γ_{tl} (i.e., the micro-slip at contacts can begin to prevail at a lower strain), a steeper decay in modulus degradation with strains $\gamma > \gamma_{tl}$, and a lower shear modulus at $\gamma > \gamma_{tl}$. These three effects indicate that adsorbed water facilitates micro-slip (or reduces friction) at particle contacts when $\gamma > \gamma_{tl}$.
- The most important effect on $G_{\max}$ (at $\gamma < \gamma_{tl}$) is observed after drying from high-to-low relative humidity (stage 2 to stage 3 in Fig. 5b—$\Delta G_{\max}/G_{\max} \sim 3.2\%$). The clear increase in small-strain stiffness during drying may result from hydrated ions (and small fines) migration towards contacting asperities and the ensuing precipitation (and flocculation) at contacts during drying (also observed in [19]).

5.4 Capillary bridge breakage: micro-scale study

The formation-breakage of capillary bridges at contacting asperities has not been previously considered and it is explored herein through micro-scale experimentation and analysis.

Experimental data are gathered by measuring the force-displacement curve experienced by a small asperity as it recedes from a mineral surface coated with water monolayers. An atomic force microscope is used for this purpose (AFM—Pico SPM by Molecular Image Company). The "asperity" is a silicon nitride Si_3N_4 tip (nominal tip diameter $d_a = 40$ nm) which is mounted on a cantilever beam with stiffness 0.58 N/m (Digital Instruments). The substrate is a freshly cleaved quartz surface. The AFM device is supported on a vibration isolation box to filter environmental noise ($\sim$ 1 Hz resonant frequency). The relative humidity inside the test chamber is controlled following a similar procedure used for resonant column specimens.

Figure 6a presents a force-distance measurement under $RH = 60\%$. Several regions are observed (see also [58,82,87]). In Region A, the tip is far from the surface and it cannot sense any force. Near the surface, the tip jumps to contact the

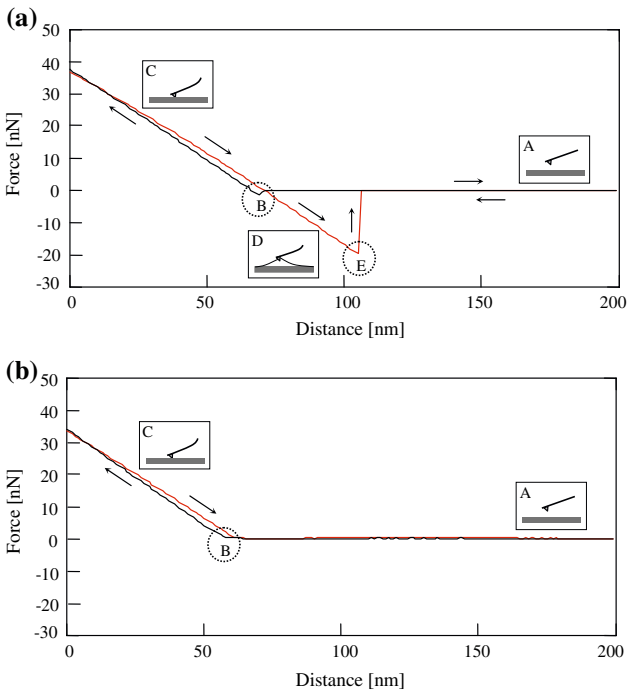

Fig. 6 Contact hysteresis due to adsorbed layers—Force-distance measurements. **a** In moist air RH = 60%. **b** Submerged in water to cancel the capillary force

substrate due to van der Waals attraction (small depression at Point B—hydration forces act near this point). In Region C, the tip penetration into the surface is opposed by the strong Born repulsion due to the overlap of the electron clouds of atoms. When the tip is retracted from the specimen, the capillary force develops as the meniscus is stretched (Regions D). The maximum withdrawal force required to separate the tip from the surface is observed at Point E and is herein called the pull-off force F. Further retraction of the tip causes the capillary bridge to break and the energy stored in the bridge is dissipated by fluid flow that follows the necking of the capillary bridge. The force-distance curve does not detect post-peak processes such as the necking of the capillary bridge because of the soft cantilever spring constant. The triangular region with base δ_r and height F captures the adhesion hysteresis.

In order to verify that the pull-off force at point E corresponds to the breakage of the capillary bridge, a test is conducted by fully immersing the tip and substrate in water to cancel the capillary force while all other forces remain. The resulting force-distance curve shown in Fig. 6b confirms the previous interpretation and does not exhibit the strong tension exerted by capillaries (the van der Waals attraction force at point B is weaker in this case because the Hamaker's constant is smaller if the intermediate medium is water instead of air [33,37]).

Hysteretic loss is measured 50 times at randomly varying locations on the substrate, for each relative humidity during a sequence of increasing and decreasing air moisture conditions. The histograms in Fig. 7 show an increase in hysteretic loss with increasing relative humidity. The relatively small changes in loss suggest a large radius "asperity" tip compared to the thickness of the water film and the possible formation of water island rather than continuous water films at low relative humidity. The average hysteretic loss in each detachment is $L_a \approx 3.4 \times 10^{-16}$ J at high relative humidity. (Note: there are similar studies in [71,73,87,88]. The magnitude of the pull-off force is comparable; however, trends are affected by tip type, substrate characteristics, tip contamination and rate of tip retraction).

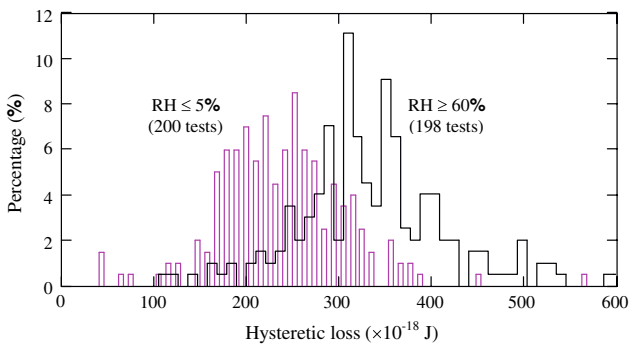

Fig. 7 Histograms of hysteretic loss in breaking a water bridge at a single asperity—AFM measurements

The macro-scale damping ratio $D = W_L/4\pi W_S$ (Eq. 1) can be estimated by assuming a Hertzian contact. The lost energy is computed as the hysteretic loss per asperity L_a times the number of asperities in the Hertzian contact: $W_L = (\pi r_c^2/d_a^2) \cdot L_a$, where r_c is the radius of the contact area and d_a is the effective distance between asperities. The stored energy in a Hertzian contact between two particle size d is $W_S = 2 \cdot N \cdot \delta/5$ where $N = d^2\sigma'$ and the Hertzian shortening $\delta = 4r_c^2/d$. Then, the damping ratio is

$$D = \frac{5}{32} \cdot \frac{L_a}{d_a^2 \cdot d \cdot \sigma'} \text{(for one particle–particle contact)} \quad (8)$$

The predicted damping ratio is $D = 0.39\%$ for the sand and test conditions in Fig. 5 ($d = 125\mu$m subjected to $\sigma' = 69$ kPa) when the AFM data is considered ($L_a = 3.4 \times 10^{-16}$ J, and $d_a \sim 40$ nm). This energy loss mechanism increases with the strain level (analytically linear at small strains—see Eq. 4), and full contact detachment (i.e., the breakage of the capillary bridge) is needed to mobilize the value predicted in Eq. 8. This takes place when $\gamma > \gamma_{tl}$, which is the same strain level when frictional loss gains relevance. Therefore, this loss mechanism will manifest as an augmentation of frictional loss.

5.5 Summary on moisture effects

Adsorbed layers cause a significant increase in damping ratio and strain-dependent changes in stiffness. Previous studies together with new experimental results and analyses permit anticipating the following potential loss mechanisms at small and intermediate strain levels in soils: distortion and motion of adsorbed layers (water and hydrated ions), hydration force hysteresis in approaching-receding contacts as a molecular level squirt flow, boundary lubrication effects on friction, altered thermoelastic relaxation due to the presence of a more conductive fluid phase, and the formation-breakage of minute capillary bridges at contacting micro-asperities. The damping ratio due to micro-capillary breakage increases with increasing RH and strain level, and decreases with increasing confinement.

6 Discussion

A summary of attenuation mechanisms for different moisture conditions is presented in Table 2. It contains the loss mechanisms previously identified in soils (and rocks but applied to soils), and those explored in this study. For completeness, the mechanisms taking place in partially saturated and saturated conditions are also shown. Although different attenuation mechanisms can take place at the same time, they only

Table 2 Summary of soil attenuation mechanisms according to moisture conditions

Dry	Air-dry (adsorbed water)	Unsaturated-saturated[c]
Small strains ($\gamma < \gamma_{tl}$)	*Small strains*	*Strain-rate dependent*
• Thermoelastic relaxation • Other suggested losses: point defect relaxations, grain boundary viscosity, dislocations	• distortion and motion of adsorbed layers (water and hydrated ions), hydration force hysteresis, altered thermoelastic relaxation	• Viscous losses and Biot relaxation[a] • Squeeze flow between grain contacts, between neighboring pores, and between compression–extension regions
Medium-to-large strains[b] ($\gamma > \gamma_{tl}$)	*Medium-to-large strains*[b] ($\gamma > \gamma_{tl}$)	• Flow due to patchy saturation
• Frictional loss at grain contacts	• Boundary lubrication effects on friction	• Gas bubble vibration
• Energy coupling (acoustic emissions, electromagnetic emissions)	• Formation–breakage of minute capillary bridges at contacting micro-asperities	

Note: [a] Biot dispersion effects can loose relevance in soils in relation to Brillouin scattering when the wavelength approaches the grain size (high relaxation frequency and low skeleton stiffness)
[b] Losses in the medium-to-large strain regime also include losses listed under small-strains
[c] Losses in unsaturated and saturated soils include losses in air-dry soils
Sources: This study and [2–5,9,10,12,13,15,20,25–27,29,30,45,48,50,54,55,60,61,63,69,70,72,76,83,85,86,90]

prevail at certain strain levels or frequency ranges. It should be noted that the non-frictional and strain-independent loss mechanisms responsible for $D_{\min}$ in dry soils are active at different strain levels and moisture conditions as background attenuation.

Attenuation implies dispersion (e.g., the material modulus becomes a function of frequency) in any linear, causal system, as prescribed in Kramers–Kronig relations [77]. Therefore, the small-strain shear modulus $G_{\max,a}$ and $G_{\max,b}$ at frequencies ω_a and ω_b are related to $D_{\min}$ as (after [53]),

$$\frac{G_{\max,a}}{G_{\max,b}} = \left[1 + \frac{2}{\pi} \cdot D_{\min} \cdot \ln\left(\frac{\omega_a}{\omega_b}\right)\right]^2$$

which becomes

$$\frac{G_{\max,a}}{G_{\max,b}} \approx 1 + 3D_{\min} \quad \text{for } \omega_a = 10\omega_b \text{ and small } D_{\min} \quad (9)$$

For example, for a dry sand with $D_{\min} \approx 0.4\%$ the corresponding modulus dispersion predicted with Eq. 9 is $\Delta G/G < 1.2\%$ for a tenfold increase in frequency; hence air-dry sands can be considered non-dispersive for practical purposes (Note: the predicted modulus dispersion in clays for a damping ratio $D_{\min} = 2\%$ is $\Delta G/G < 6\%$ per log cycle). These observations explain experimental trends regarding frequency effects on $G_{\max}$ indicated in Table 1.

7 Conclusions

The small-strain damping ratio $D_{\min}(\gamma < \gamma_{tl})$ in air-dry sands is small-but not null, and it is essentially independent of strain and confinement. These macroscopic observations and insufficient interparticle deformation required to break inter-atomic bonds indicate that the small-strain damping in soils is non-frictional.

In part, the confusion about low-strain loss mechanisms has been sustained by the counter emf bias in resonant column testing that has affected most published soil attenuation data.

In agreement with previous studies on losses in continuous materials, thermoelastic loss is suggested to account for small-strain energy loss in air-dry soils. While thermoelastic relaxation is inherently frequency dependent, soils exhibit multiple internal scales (contact size, particle size, quasi-fractal particle chain lengths) and associated thermal diffusion lengths and time scales, so that the superposition of these relaxations can explain the nearly frequency independent $D_{\min}$ response observed in the frequency range of engineering interest.

Adsorbed water layers on grain surfaces can cause an appreciable effect on damping ratio and smaller relative change in stiffness. The damping ratio increases with increasing relative humidity.

The breakage of water bridges between contacting asperities contributes adhesion hysteresis and energy loss; however, bridge breakage is strain dependent and it is fully mobilized as the strain level approaches γ_{tl}. Other loss mechanisms must be responsible for the effect of relative humidity on small strain $D_{\min}$. These may include distortion and motion of adsorbed layers and hydration force hysteresis.

Assuming a nearly frequency-independent $D_{\min}$, under the constraint of the Kramers–Kronig relations, the associated shear modulus increases by a factor $\sim 3D_{\min}$ for every tenfold increase in frequency. For air-dry sands the predicted dispersion is low, typically about 1% per log cycle. Hence,

the medium can be considered non-dispersive for practical purposes.

Acknowledgments This research was supported by the National Science Foundation (research on seismic attenuation), the Mid America Earthquake Center (research on site response), and the Research Grants Council (HKUST6034/02E), Hong Kong.

References

1. Andersland, O., Ladanyi, B.: Frozen Ground Engineering, 2nd edn. Wiley in cooperation with ASCE Press, New York (2004)
2. Anderson, A.L., Hampton, L.D.: Acoustics of gas-bearing sediments. I. Background. J. Acoust. Soc. Am. **67**(5), 1865–1889 (1980)
3. Anderson, A.L., Hampton, L.D.: Acoustics of gas-bearing sediments. II. Measurements and models. J. Acoust. Soc. Am. **67**(5), 1890–1903 (1980)
4. Armstrong, B.H.: Frequency-independent background internal friction in heterogeneous solids. Geophysics **45**(5), 1042–1054 (1980)
5. Armstrong, B.H.: Model for thermoelastic attenuation of waves in heterogeneous solids. Geophysics **49**(6), 1032–1040 (1984)
6. Avramidis, A.S., Saxena, S.K.: The modified stiffened Drnevich resonant column apparatus. Jpn Soc. Soil Mech. Foundation Eng. **30**(3), 53–68 (1990)
7. Bhushan, B., Israelachvili, J.N., Landman, U.: Nanotribology: friction, wear and lubrication at the atomic scale. Nature **374**(13), 607–616 (1995)
8. Binggeli, M., Mate., C.M.: Influence of capillary condensation of water on nanotribology studied by force microscopy. Appl. Phys. Lett. **65**, 415–417 (1994)
9. Biot, M.A.: The theory of propagation of elastic waves in a fluid-saturated solid. I. Lower frequency range. J. Acoust. Soc. Am. **28**, 168–178 (1956)
10. Biot, M.A.: The theory of propagation of elastic waves in a fluid-saturated solid. II. Higher frequency range. J. Acoust. Soc. Am. **28**, 179–191 (1956)
11. Bocquet, L., Charlaix, E., Ciliberto, S., Crassous, J.: Moisture-induced ageing in granular media and the kinetics of capillary condensation. Nature **396**, 735–737 (1998)
12. Bolton, M.D., Wilson, J.N.: Soil stiffness and damping. In: Krätzig, et al. (eds.) Structural Dynamics: Proceedings of the European Conference on Structural Dynamics, Eurodyn '90, pp. 209–216. Balkema, Rotterdam (1990)
13. Bourbié, T., Coussy, O., Zinszner, B.: Acoustics of Porous Media. Gulf Publishing Co., Houston (1987)
14. Brunauer, S., Emmett, P.H., Teller, E.: Adsorption of gases in multimolecular layers. J. Am. Chem. Soc. **60**, 309–319 (1938)
15. Cascante, G, Santamarina, J.C., Yassir, N.: Flexural excitation in a standard torsional-resonant column device. Can. Geotech. J. **35**, 478–490 (1998)
16. Cascante, G., Santamarina, J.C.: Interparticle contact behavior and wave propagation. J. Geotech. Geoenviron. Eng. **122**, 831–839 (1996)
17. Cascante, G., Stantamarina, J.C.: Low strain measurements using random noise excitation. Geotech. Testing J. **20**(1), 29–39 (1997)
18. Cascante, G., Vanderkooy, J., Chung, W.: Difference between current and voltage measurement in resonant-column testing. Can. Geotech. J. **40**, 806–820 (2003)
19. Cho, G.C., Santamarina, J.C.: Unsaturated particulate materials-particle-level studies. J. Geotech. Geoenviron. Eng. **127**, 84–96 (2001)
20. Clark, V.A., Tittmann, B.R., Spencer, T.W.: Effect of volatiles on attenuation (Q^{-1}) and velocity in sedimentary rocks. J. Geophys. Res. **85**, 5190–5198 (1980)
21. Clifford, J.: Properties of water in capillaries and thin film. In: Franks, F. (ed.) Water-A Comprehensive Treatise, vol 5, pp 75–132. Plenum Press, New York (1975)
22. Clough, R.W., Penzien, J.: Dynamics of Structures, 2nd edn. McGraw-Hill Inc., New York (1993)
23. Dini, D., Nowell., D.: Prediction slip zone friction coefficient in flat and rounded contact. Wear **254**, 363–369 (2003)
24. Dobry, R., Vucetic, M.: Dynamic properties and seismic response of soft clay deposits. In: Mendoza, M., Montanez, L. (eds.) Proceedings of the International Symposium on Geotechnical Engineering of Soft Soils, Mexico City, vol. 2, pp. 51–87 (1987)
25. Dobry, R., Ladd, R.S., Yokel, F.Y., Chung, R.M., Powell, D.: Prediction of Pore Water Pressure Buildup and Liquefaction of Sands during Earthquakes by the Cyclic Strain Method. (National Bureau of Standards Building Science Series 138, U.S. Government Printing Office, Washington (1982))
26. Ellis, E.A., Soga, K., Bransby, M.F., Sato, M.: Resonant column testing of sands with different viscosity pore fluids. J. Geotech. Geoenviron. Eng. **126**(1), 10–17 (2000)
27. Fratta, D.: Passive and Active Measurements of Unique Phenomena in Geotechnical Engineering. PhD Thesis, Georgia Institute of Technology, USA (1999)
28. Frocht, M.M.: Photoelasticity. Wiley, New York (1941)
29. García-Rojo, R., Herrmann, H.J.: Shakedown of unbound granular material. Granular Matter **7**, 109–118 (2005)
30. Gudehus, G.: Seismo-hypoplasticity with a granular temperature. Granular Matter **8**, 93–102 (2006)
31. Hardin, B.O., Drnevich, V.P.: Shear modulus and damping in soils: measurement and parameter effects. J. Soil Mech. Foundation Eng. **98**, 603–624 (1972)
32. Hardin, B.O.: The nature of damping in sands. J. Soil Mech. Foundation Division ASCE **91**, 63–97 (1965)
33. Hartmann, U.: Fundamental and special applications of non-contact scanning force microscopy. Adv. Electron. Electro Phys. **87**, 79–200 (1994)
34. Homola, A.M., Israelachvili, J.N., Gee, M.L., Mcguiggan, P.M.: Measurements of and relation between the adhesion and friction of two surfaces separated by molecularly thin liquid films. J. Tribol. Trans. ASME **111**(4), 675–682 (1989)
35. Hu, J., Xiao, X.D., Ogletree, D.F., Salmeron, M.: Atomic scale friction and wear of mica. Surface Sci. **327**, 358–370 (1995)
36. Ishihara, K.: Soil Behavior in Earthquake Geotechnics. Oxford Science, Oxford (1996)
37. Israelachvili, J.: Intermolecular and Surface Forces, 2nd edn. Academic, New York (1991)
38. Israelachvili, J., Wennerström, H.: Role of hydration and water structure in biological and colloidal interactions. Nature **379**, 219–225 (1996)
39. Johnson, K.L.: Energy dissipation at spherical surfaces in contact transmitting oscillating forces. J. Mech. Eng. Sci. **3**(4), 362–368 (1961)
40. Johnson, K.L.: Contact Mechanics. Cambridge University Press, New York (1984)
41. Johnston, D.H.: Attenuation: a state-of-the-art summary. In: Toksöz, M.N., Johnson, D.H (eds.) Seismic Wave Attenuation, pp. 123–135. SEG Geophysics Reprint Series (1981)
42. Kim, D.S., Stokoe, K.H., Hudson, W.R.: Deformational Characteristics of Soils at Small to Intermediate Strains from Cyclic Tests. Report 1177-3. (Center for Transportation Research, Bureau of Engineering Research, the University of Texas Austin, 1991)
43. Kjartansson, E.: Constant Q—wave propagation and attenuation. J. Geophys. Res. **84**(B9), 4737–4748 (1979)

44. Klimentos, K.: Attenuation of P- and S-waves as a method of distinguishing gas and condensate from oil and water. Geophysics **60**, 447–458 (1995)
45. Knight, R., Dvorkin, J.: Seismic and electrical properties of sandstones at low saturations. J. Geophys. Res. **97**(B12), 17425–17432 (1992)
46. Kokusho, T.: Cyclic triaxial test of dynamic soil properties for wide strain range soils and foundations **20**, 45–60 (1980)
47. Kramer, S.L.: Geotechnical Earthquake Engineering. Prentice Hall, New Jersey (1996)
48. Landman, U., Luedtke, W.D., Gao, J.P.: Atomic-scale issues in tribology: interfacial junctions and nano-elastohydrodynamics. Langmuir **12**, 4514–4528 (1996)
49. Latham, G., Ewing, M., Dorman, J., Press, F., Tokoz, N., Sutton, G., Meissner, R., Duennebier, F., Nakamura, Y., Kovach, R., Yates, M.: Reports: seismic data from man-made impacts on the moon. Science **170**, 620–626 (1970)
50. Lazan, B.J.: Damping of Materials and Members in Structural Mechanics. Pergamon Press, New York (1968)
51. Li, W.L., Yang, X.S.: Effects of vibration history on modulus and damping of dry sand. J. Geotech. Geoenviron. Eng. **124**(11), 1071–1081 (1998)
52. Li, X.S., Yang, W.L., Shen, C.K., Wang, W.C.: Energy-injecting virtual mass resonant column system. J. Geotech. Geoenviron. Eng. **124**, 428–438 (1998)
53. Liu, H.P., Anderson, D.L., Kanamori, H.: Velocity dispersion due to anelasticity; implications for seismology and mantle composition. Geophys. J. R. Astron. Soc. **47**, 41–58 (1976)
54. Mavko, G., Nur, A.: Melt squirt in the asthenosphere. J. Geophys. Res. **80**(11), 1444–1448 (1975)
55. Mavko, G., Nur, A.: Wave attenuation in partially saturated rocks. Geophysics **44**(2), 161–178 (1979)
56. Mavko, G., Kjartansson, E., Winkler, K.: Seismic wave attenuation in rocks. Rev. Geophys. Space Phys. **17**(5), 1155–1164 (1979)
57. Meng, J., Rix, G.J.: Reduction of equipment-generated damping in resonant column measurements. Géotechnique **53**(4), 503–512 (2003)
58. Meyer, E., Heinzelmann, H. : Scanning force microscopy (SFM). In: Wiesendanger, R., Güntherodt, H.J. (eds.) Scanning Tunneling Microscopy II., pp. 99–149. Springer-Verlag, Berlin (1992)
59. Murphy III, W.F., Winkler, K.W., Klinberg, R.L.: Frame modulus reduction in sedimentary rocks: the effect of adsorption on grain contacts. Geophys. Res. Lett. **1**(9), 805–808 (1984)
60. Murphy III, W.F., Winkler, K.W., Kleinberg, R.L.: Acoustic relaxation in sedimentary rocks: dependence on grain contacts and fluid saturation. Geophysics **51**, 757–766 (1986)
61. Murphy III, W.F.: Effects of partial water saturation on attenuation in Massilon sandstone and Vycor porous glass. J. Acoust. Soc. Am. **71**(5), 1458–1468 (1982)
62. Nowick, A.S., Berry, B.S.: Anelastic Relaxation in Crystalline Solids. Academic, New York (1972)
63. O'Connell, R.J., Budiansky, B.: Viscoelastic properties of fluid-saturated cracked solids. J. Geophys. Res. **82**(36), 5719–5735 (1977)
64. Parks, G.A.: Surface and interfacial free energies of quartz. J. Geophys. Res. **89**(B6), 3997–4008 (1984)
65. Persson, B.N.J.: Sliding Friction, Physical Principles and Applications, 2nd edn. Springer, New York (2000)
66. Radjai, F., Wolf, D.E., Jean, M., Moreau, J.J.: Biomodal character of stress transmission in granular packing. Phys. Rev. Lett. **80**(1), 61–64 (1998)
67. Richart, F.E. Jr., Hall, J.R., Woods, R.D.: Vibrations of Soils and Foundations. Prentice-Hall, Inc., Englewood Cliffs (1970)
68. Santamarina, J.C., Cascante, G.: Stress anisotropy and wave propagation: a micromechanical view. Can. Geotech. J. **33**(4), 770–782 (1996)
69. Santamarina, J.C., Klein, K.A., Fam, M.A.: Soils and Waves. Wiley, New York (2001)
70. Savage, J.C.: Attenuation of elastic waves in granular mediums. J. Geophys. Res. **70**(16), 3935–3942 (1965)
71. Sedin, D., Rowlen, K.L.: Adhesion forces measured by atomic force microscopy in humid air. Anal. Chem. **72**(10), 2183–2189 (2000)
72. Spencer, J.W.: Stress relaxations at low frequencies in fluid-saturated rocks: attenuation and modulus dispersion. J. Geophys. Res. **86**, 1803–1812 (1981)
73. Thundat, T., Zheng, X.Y., Chen, G.Y., Warmack, R.J.: Role of relative humidity in atomic force microscopy imaging. Surface Sci. Lett. **294**, L939–L943 (1993)
74. Tittmann, B.R.: Lunar rock seismic Q in 3000–5000 range achieved in laboratory. Phil. Trans. R. Soc. Lond. A **285**, 475–479 (1977)
75. Tittmann, B.R., Abdel-Gawad, M., Housley, R.M.: Elastic velocity and Q measurements on Apollo 12, 14, and 15 rocks. In: Proc. Lunar Sci. Conf. 3rd, pp. 2565–2575. MIT Press, Cambridge (1972)
76. Tittmann, B.R., Clark, V.A., Richardson, J.M., Spencer, T.W.: Possible mechanism for seismic attenuation in rocks containing small amounts of volatiles. J. Geophys.l Res. **85**(B10), 5199–5208 (1980)
77. Toll, J.S.: Causality and the dispersion relation: logical foundations. Phys. Rev. **104**(5), 1760–1770 (1956)
78. Vucetic, M., Dobry, R.: Effect of soil plasticity on cyclic response. J. Geotech. Eng. **117**(1), 89–107 (1991)
79. Vucetic, M.: Cyclic threshold shear strains in soils. J. Geotech. Eng. **120**(12), 2208–2227 (1994)
80. Wang, Y.H.: Attenuation in Soils and Non-linear Dynamic Effects. PhD Thesis, Georgia Institute of Technology, USA (2001)
81. Wang, Y.H., Cascante, G., Santamarina, J.C.: Resonant column testing: the inherent counter emf effect. ASTM Geotech. Testing J. **26**(3), 342–352 (2003)
82. Weisenhorn, A.L., Hansma, P.K., Albrecht, T.R., Quate, C.F.: Forces in atomic force microscopy in air and water. Appl. Physics Letter **54**(26), 2651–2653 (1989)
83. White, J.E.: Computed seismic speeds and attenuation in rocks with partial gas saturation. Geophysics **40**, 224–232 (1975)
84. Winkler, K.W., Murphy III, W.F.: Acoustic Velocity and Attenuation in Porous Rocks. In: Ahrens, T.J. (ed.) Rock Physics & Phase Relations—A Handbook of Physical Constants. AGU Reference Shelf 3, pp. 20–34 (1995)
85. Winkler, K., Nur, A., Gladwin, M.: Friction and seismic attenuation in rocks. Nature **227**, 528–531 (1979)
86. Winkler, K.W., Nur, A.: Seismic attenuation: effects of pore fluids and frictional sliding. Geophysics **47**(1), 1–15 (1982)
87. Xiao, X., Qian, L.: Investigation of humidity-dependent capillary force. Langmuir **16**, 8153–8158 (2000)
88. Xu, L., Lio, A., Hu, J., Ogletree, D.F., Salmeron, M.: Wetting and capillary phenomena of water on mica. J. Phys. Chem. B **102**, 540–548 (1998)
89. Yoshizawa, H., Chen, Y.L., Israelachvili, J.: Fundamental mechanisms of interfacial friction. J. Phys. Chem. **97**, 4128–4140 (1993)
90. Zener, C.: Elasticity and Anelasticity of Metals. The University of Chicago Press, Chicago (1948)